Journal of Sedimentary Research

Journal of Sedimentary Research, 2006, v. 76, 605–617
Research Article
DOI: 10.2110/jsr.2006.050

REE AND Nd ISOTOPE STRATIGRAPHY OF A LATE JURASSIC CARBONATE PLATFORM, EASTERN PARIS BASIN, FRANCE

PHILIPPE NÉGREL,[1] JOEL CASANOVA,[1] AND JACQUES BRULHET[2]
[1]*BRGM, Avenue C. Guillemin, BP 6009, 45060 Orleans Cedex 02, France*
[2]*ANDRA, 1, rue Jean Monnet, 92290 Chatenay-Malabry Cedex, France*
e-mail: p.negrel@brgm.fr

ABSTRACT: **Rare earth elements (REE) and Nd isotopes on the labile fraction of the Callovian–Oxfordian to Tithonian Jurassic carbonate platform of the eastern Paris Basin were used to reconstruct the composition of the contemporaneous waters from which the labile fraction may have originated. This sedimentary record shows a remarkable change in the manganese content between the clayey deposits at the top and bottom of the succession and the carbonate-platform deposits. The combined analyses of REE and Nd isotope ratios record the influence of emerged land and the Tethys Ocean. The REE patterns are similar to those of seawater in the middle part of the sedimentary record, suggesting REE removal by marine carbonate, while bell-shaped REE patterns are observed above and below, reflecting continent-derived REE carried by Fe–Mn coatings on detrital particles. Therefore, the REE patterns and their evolution through the sedimentary record highlight the roles played in the REE budget by Fe–Mn coatings on detrital particles and by marine carbonates. The predominant sources of Nd during platform evolution are characterized by the Nd isotope variations in the sediments; the nonradiogenic values ($\varepsilon Nd_{(t)}$ between −12 and −10) strongly suggest that the predominant source of Nd on the platform was the continental crust through weathering and river inputs, whereas some more radiogenic Nd ($\varepsilon Nd_{(t)} = -5$) values are more typical of the Tethys seawater signature.**

INTRODUCTION

Radiogenic isotopes such as lead, neodymium, and strontium are especially suitable for determining the provenance of inputs to the ocean (Dia et al. 1992; Frank et al. 1999; Fanton et al. 2002). Their dominant sources are the continents, and they are present in seawater as dissolved and particulate loads that have been supplied to the oceans by rivers and winds and then further transported by currents and sinking particles (Ehrenberg et al. 2000; Fanton et al. 2002).

Because dissolved Nd has a short residence time in seawater (~ 200–1000 years) compared to the oceanic mixing time (~ 1500 years), it is not isotopically homogeneous throughout the ocean. Consequently, each water mass possesses its own unique isotopic signature (Piepgras and Wasserburg 1980; Tachikawa et al. 1999a). Recent results in paleoceanography have been obtained using the Nd isotope composition of Fe–Mn crust, shells, and fish teeth (Holmden et al. 1996; Rutberg et al. 2000; Martin and Haley 2000), leading to the use of Nd isotopes as a stratigraphic tool (Martin and MacDougall 1995; Ehrenberg et al. 2000). Records of water-derived Nd onto Fe–Mn crust generally give evidence for the long-term evolution of water-mass composition, related to the opening of oceanic gateways (Frank et al. 1999).

Concentrations, as well as patterns of rare earth elements (REE), provide an important body of information on marine depositional environments (Elderfield et al. 1981; Palmer and Elderfield 1986; Banner et al. 1988; Bellanca et al. 1997). REE are usually used as tracers of biogenic and continental fluxes (Piper 1974; Amakawa et al. 2000), and the chemical characteristics of REE in seawater have been applied in paleoceanography using the REE content of marine biogenic phosphates of Phanerozoic age to discuss the identification of distinct water masses and the influence of detrital REE inputs on the REE budget of coastal waters (Grandjean et al. 1988), and the secular evolution of the REE contents of the world's oceans (Grandjean-Lécuyer et al. 1993). Among the REEs, cerium has been used as a tracer of paleo–oceanic redox conditions (Wright and Holsen 1987; Wang et al. 1993; Bellanca et al. 1997).

Here, we used a leaching procedure that produces the separation of a labile fraction (e.g., Fe–Mn oxide, carbonate, elements adsorbed onto clays, etc., according to Négrel et al. 2000a) from a sediment sample, the labile fraction being suitable for REE and Nd isotope analysis (Bros et al. 1992; Clauer et al. 1993; Schaltegger et al. 1994; Freydier et al. 2001; Bayon et al. 2002). For any given sample, this procedure allows the Nd isotopes and REE patterns to be used as proxies, i.e., the chemical and isotopic composition of the labile component as a direct record of the contemporaneous composition of the water(s) from which they originated (Bayon et al. 2002; Fanton et al. 2002; Négrel et al. 2000a).

A record of REE data and Nd isotope ratios covering the Callovian–Oxfordian to Tithonian times of the Jurassic carbonate platform of the eastern Paris Basin is presented. The results of the combined analyses on the labile fraction precisely characterize and constrain sediment provenance related to neighboring land and the Tethys Ocean.

GEOLOGICAL SETTING OF THE SEDIMENTARY BASIN: LITHOLOGICAL CHARACTERIZATION OF THE FORMATIONS

The Paris Basin, which extends over some 135,000 km^2, contains a sedimentary succession more than 3000 m thick that represents

 1527-1404/06/076-605/$03.00

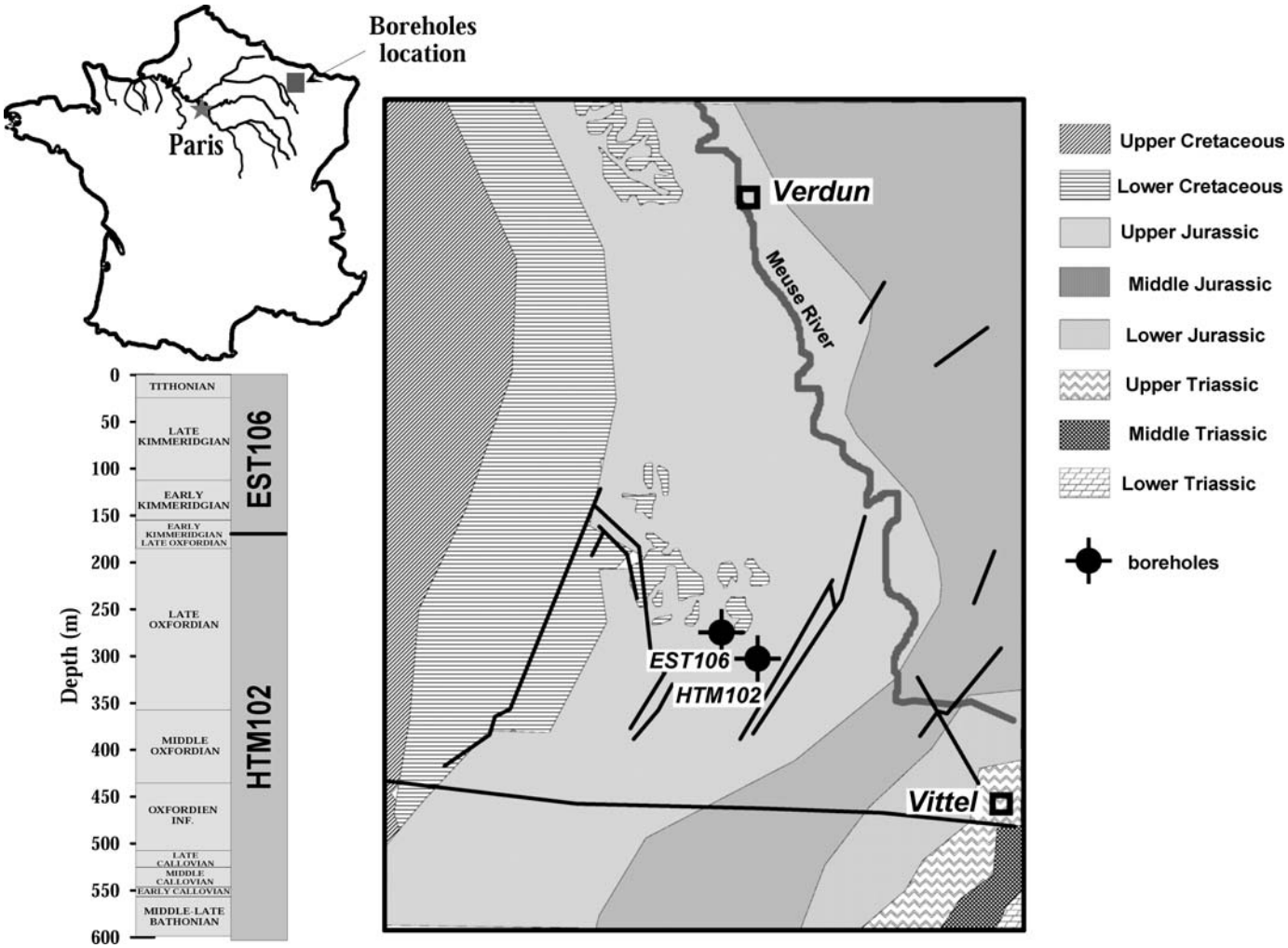

FIG. 1.—Site location in the eastern Paris Basin, lithological log, and simplified geological map.

deposition in a stable-shelf basin from the Triassic to the Cenozoic (Fig. 1A; Guillocheau et al. 2000). The present-day Paris Basin is surrounded by Cadomian–Variscan basement massifs; i.e., the Armorican Massif to the west, the Massif Central to the south, the Vosges to the east, and the Ardennes to the northeast (BRGM 1996). Nine major sedimentary cycles have been identified from the Triassic to the early Late Cretaceous (Guillocheau et al. 2000). Among these, the Early Bathonian–Oxfordian cycle is characterized by the end of the Bathonian aggradational carbonate platform, with shoals and carbonate muds being deposited in a protected marine environment.

The eastern Paris Basin is made up of Jurassic shelf carbonates of Late Bathonian–Callovian to Tithonian age (Dagallier et al. 2000). Bathonian sedimentation has the major features typical of the Middle Jurassic: a broad shallow-water carbonate platform (oolitic to gravelly bioclastic facies) with a relatively low detrital input. The Middle Callovian–Early Oxfordian succession is composed of argillite, representing the sedimentation of detrital clays by simple aggradation processes (Pellenard et al. 1999). It corresponds to monotonous clayey sedimentation, marked by the deposition of gray-black, finely bioclastic silty-calcareous argillite. The detrital clays may have originated from soils and alterites reflecting erosion processes on the emerged continents of the Brabant Massif, the Armorican Massif, and the Massif Central (Ziegler 1988). The Callovo–Oxfordian formation can be presented as a complex mineral assemblage of quartz, feldspars, phyllosilicates, and clays (kaolinite, illite, montmorillonite) with small amounts of Fe-minerals (pyrite, siderite) and Fe oxyhydroxides (Vieillard et al. 2004). The Middle Oxfordian marked the beginning of carbonate progradation; sedimentation corresponded to reefal deposits between an open-marine domain to the west and a lagoonal domain to the east. The Late Oxfordian is marked by micritic then biohermal limestone (Dagallier et al. 2000). The Late Oxfordian platform comprises reefal mounds with a relatively high detrital flux originating from areas located to the east. Some washover fans and/or storm deposits are observed (Dagallier et al. 2000). The Late Oxfordian–Early Kimmeridgian corresponded to shoals and reefal deposits, typical of the inner platform (infralittoral to distal system). Weathering on the emerged part of the continent was intense, as reflected by the increased clay content and by the changes in the clay mineralogy. A transgressive phase with clayey sedimentation in deeper-water conditions occurred in the Late Kimmeridgian. The Tithonian reflects the major Late Jurassic regression with limestone deposits.

MATERIALS AND METHODS

Materials

The Callovian–Oxfordian clay layer has been investigated by drilling, from which two cored boreholes (HTM102 and EST106)

TABLE 1.—*REE systematics in the labile fraction AEM.*

Samples	Depth (m)	La (μg g^{-1})	Ce (μg g^{-1})	Pr (μg g^{-1})	Nd (μg g^{-1})	Sm (μg g^{-1})	Eu (μg g^{-1})	Gd (μg g^{-1})	Tb (μg g^{-1})	Dy (μg g^{-1})	Ho (μg g^{-1})	Er (μg g^{-1})	Tm (μg g^{-1})	Yb (μg g^{-1})	Lu (μg g^{-1})	ΣREE (μg g^{-1})	Mn (μg g^{-1})	$^{143}Nd/^{144}Nd$ ± 2σ	ε $Nd_{(0)}$	ε $Nd_{(t)}$
EST106																				
EST3330	10.08	1.87	3.25	0.42	1.62	0.32	0.08	0.33	0.05	0.31	0.06	0.16	0.02	0.12	0.019	8.62	75.0	0.512079 ± 5	−10.87 ± 0.1	−9.39
EST3334	20.42	3.31	5.82	0.76	3.010	0.64	0.15	0.70	0.10	0.61	0.11	0.32	0.04	0.25	0.037	15.86	131.0	—	—	—
EST3338	29.95	10.70	18.70	2.73	11.00	2.21	0.53	2.18	0.31	1.77	0.34	0.90	0.12	0.69	0.098	52.28	137.0	—	—	—
EST1298	40.08	21.20	44.00	6.01	24.80	5.14	1.19	4.95	0.70	3.78	0.68	1.71	0.22	1.19	0.160	115.73	225.0	0.512069 ± 4	−11.06 ± 0.08	−9.70
EST3341	50.55	8.21	14.10	1.99	7.99	1.61	0.38	1.71	0.24	1.43	0.28	0.73	0.1	0.59	0.078	39.44	146.0	—	—	—
EST3342	59.98	13.10	25.20	3.36	13.40	2.73	0.64	2.72	0.40	2.16	0.40	1.05	0.14	0.83	0.120	66.25	253.0	0.512092 ± 4	−10.61 ± 0.08	−9.21
EST3345	69.88	5.20	7.67	1.07	4.06	0.72	0.17	0.74	0.10	0.57	0.11	0.30	0.04	0.22	0.032	21.00	125.0	—	—	—
EST3348	80.00	1.23	1.66	0.21	0.82	0.15	0.04	0.19	0.02	0.14	0.03	0.08	0.01	0.05	0.008	4.64	82.0	—	—	—
EST3349	90.13	13.30	24.00	3.33	13.30	2.55	0.57	2.27	0.32	1.69	0.31	0.83	0.10	0.62	0.087	63.28	223.0	0.512085 ± 10	−10.75 ± 0.2	−9.21
EST3351	100.03	16.80	35.20	4.66	19.00	4.08	0.92	3.87	0.54	2.88	0.51	1.33	0.17	0.98	0.140	91.08	257.0	—	—	—
EST3356	109.96	3.69	5.74	0.80	3.09	0.60	0.14	0.65	0.09	0.52	0.10	0.29	0.04	0.23	0.034	16.01	100.0	—	—	—
EST1472	120.03	17.40	34.60	4.42	17.90	3.60	0.87	3.60	0.49	2.75	0.50	1.28	0.17	0.94	0.130	88.65	372.0	0.512089 ± 4	−10.67 ± 0.08	−9.24
EST3359	129.83	2.12	3.65	0.49	1.90	0.37	0.09	0.40	0.06	0.31	0.06	0.16	0.02	0.12	0.019	9.76	123.0	—	—	—
EST3360	140.30	1.68	3.32	0.42	1.67	0.35	0.08	0.32	0.04	0.27	0.05	0.13	0.02	0.11	0.019	8.47	72.0	0.512074 ± 10	−10.96 ± 0.2	−9.63
EST3364	149.84	1.99	4.06	0.53	2.03	0.42	0.09	0.37	0.06	0.31	0.06	0.16	0.02	0.13	0.019	10.25	58.0	—	—	—
HTM102																				
HTM 2777	158.05	1.32	2.82	0.35	1.38	0.29	0.07	0.30	0.04	0.23	0.04	0.11	0.01	0.1	0.013	7.07	58.4	0.512122 ± 18	−10.03 ± 0.36	−8.70
HTM 2781	200.41	0.32	0.18	0.04	0.13	0.03	*ld*	0.06	*ld*	0.05	0.01	0.04	0.005	0.03	0.006	*0.90*	13.2	0.512298 ± 12	−6.59 ± 0.24	−5.50
HTM 2783	207.90	0.07	0.05	0.01	0.04	0.01	0.005	0.02	0.005	0.01	0.004	0.01	0.003	*ld*	0.004	*0.25*	11.8	0.512033 ± 40	−11.76 ± 0.8	−10.63
HTM 2785	219.75	0.34	0.36	0.04	0.17	0.04	0.01	0.06	0.01	0.04	0.01	0.04	0.006	0.02	0.006	*1.15*	96.4	0.512044 ± 20	−11.55 ± 0.4	−10.51
HTM 2788	238.35	1.56	1.57	0.27	1.06	0.22	0.05	0.250	0.034	0.24	0.05	0.16	0.02	0.12	0.021	5.63	38.4	0.512125 ± 11	−9.97 ± 0.22	−8.61
HTM 2792	270.00	0.51	0.29	0.05	0.21	0.04	*ld*	0.06	*ld*	0.05	0.01	0.05	0.006	0.04	0.005	*1.31*	23.6	0.512123 ± 7	−10.01 ± 0.14	−8.50
HTM 2796	288.01	0.07	0.04	0.01	0.04	0.02	0.008	0.02	0.004	0.02	0.004	0.01	0.004	*ld*	0.004	*0.26*	5.8	0.512061 ± 15	−11.22 ± 0.3	−11.40
HTM 2799	305.25	0.06	0.01	*ld*	0.01	*ld*	*ld*	*ld*	*ld*	*ld*	*ld*	*ld*	*ld*	0.01		*0.09*	5.8	0.512284 ± 50	−6.87 ± 1	—
HTM 2801	318.24	0.10	0.04	0.01	0.06	0.03	0.01	0.03	0.004	0.02	0.006	0.015	0.003	0.02	0.006	*0.36*	6.6	0.512133 ± 9	−9.81 ± 0.18	−11.48
HTM 2805	337.37	0.35	0.12	0.03	0.13	0.02	*ld*	0.03	*ld*	0.03	0.006	0.025		0.02	0.003	*0.78*	10.6	0.512126 ± 11	−9.95 ± 0.22	−8.32
HTM2845	355.68	0.08	0.02	0.01	0.03	0.01	*ld*	*0.010*	*ld*	0.01	0.003	*ld*	0.002	*ld*	0.001	*0.17*	8.1	0.512052 ± 50	−11.39 ± 1	−11.04
HTM 2809	363.20	3.76	1.17	0.41	1.67	0.26	0.05	0.34	0.03	0.27	0.06	0.17	0.020	0.12	0.016	8.35	18.8	0.512197 ± 5	−8.56 ± 0.1	−6.60
HTM 2813	378.03	0.38	0.10	0.04	0.16	0.05	0.01	0.06	0.007	0.04	0.01	0.04	0.005	0.03	0.006	0.94	13.5	0.512189 ± 7	−8.72 ± 0.14	−8.58
HTM 2816	393.19	0.33	0.15	0.03	0.14	0.03	*ld*	0.03	*ld*	0.03	0.01	0.02	*ld*	0.02	0.003	*0.79*	25.6	0.512189 ± 13	−8.72 ± 0.26	−7.27
HTM616	409.41	5.82	3.51	0.73	2.94	0.41	0.09	0.52	0.05	0.34	0.07	0.19	0.02	0.12	0.015	14.82	60.5	0.512158 ± 11	−9.32 ± 0.22	−7.18
HTM80619	417.56	22.40	27.90	4.19	15.30	2.47	0.56	2.50	0.31	1.59	0.29	0.74	0.09	0.54	0.075	78.96	177.0	0.512108 ± 5	−10.30 ± 0.1	−8.41
HTM621	428.08	17.00	23.90	3.61	13.80	2.42	0.55	2.41	0.31	1.58	0.29	0.75	0.09	0.53	0.075	67.32	207.0	0.512105 ± 6	−10.36 ± 0.12	−8.63
HTM856	446.56	23.90	42.00	6.31	26.40	5.05	1.01	3.74	0.490	2.480	0.48	1.17	0.150	0.780	0.110	114.07	288.0	0.512058 ± 3	−11.28 ± 0.06	−9.73
HTM 80665	448.84	14.60	19.50	2.72	10.60	1.80	0.39	1.74	0.210	1.080	0.19	0.47	0.064	0.360	0.047	53.77	242.0	0.512056 ± 5	−11.31 ± 0.1	−9.52
HTM 918	459.40	19.90	33.30	4.43	18.10	3.23	0.67	2.70	0.340	1.790	0.33	0.82	0.100	0.580	0.082	86.37	287.0	0.512059 ± 5	−11.26 ± 0.1	−9.56
HTM 1017	484.53	10.80	16.00	1.90	7.25	1.04	0.25	1.21	0.150	0.760	0.15	0.39	0.045	0.240	0.036	40.22	540.0	0.512077 ± 5	−10.90 ± 0.1	−8.80
HTM630	505.08	29.60	58.20	7.09	26.10	5.32	1.31	5.50	0.730	3.500	0.60	1.52	0.210	1.200	0.160	141.04	500.0	0.512052 ± 5	−11.39 ± 0.1	−9.99
HTM598	515.54	10.40	9.49	1.56	6.01	0.89	0.20	0.96	0.120	0.630	0.13	0.34	0.039	0.200	0.030	31.00	226.0	0.512094 ± 4	−10.57 ± 0.08	−8.52
HTM 1177	523.86	14.70	16.20	2.51	9.80	1.50	0.32	1.53	0.180	0.930	0.18	0.45	0.056	0.300	0.042	48.70	181.0	0.512029 ± 6	−11.84 ± 0.12	−9.85
HTM632	528.39	23.00	37.10	6.01	23.60	4.26	0.97	3.99	0.520	2.700	0.48	1.18	0.150	0.870	0.120	104.95	197.0	0.512031 ± 6	−11.80 ± 0.12	−10.13
HTM636	547.08	0.72	0.84	0.14	0.57	0.10	0.03	0.12	0.016	0.087	0.02	0.05	0.006	0.038	0.007	2.73	221.0	0.512064 ± 6	−11.16 ± 0.12	−9.43
HTM 2822	556.90	7.88	10.90	1.42	5.58	1.14	0.29	1.44	0.190	1.010	0.21	0.56	0.082	0.490	0.064	31.26	235.0	0.512087 ± 5	−10.71 ± 0.1	−9.31
HTM 2825	567.10	1.96	2.52	0.36	1.46	0.28	0.07	0.37	0.050	0.300	0.06	0.17	0.021	0.120	0.019	7.76	123.0	0.512078 ± 6	−10.88 ± 0.12	−9.34

Elemental REE and ΣREE contents (μg/g); *ld* indicates data below the detection limit and no entry indicates non-determined values. $^{143}Nd/^{144}Nd$ ratios, ε$Nd_{(0)}$ and ε$Nd_{(t)}$, are also shown.

served as the support for this study. The samples were selected from the HTM102 and EST106 cores on either side of the interface between the clay formation and the carbonate rocks, i.e., on the maximum flooding surfaces characterized by peaks in clay content, and on the progradation maxima characterized by carbonate peaks (Pellenard et al. 1999; Andra 2001). A total of 42 samples from these cores was collected for REE determination and Nd isotopic analysis (Table 1).

Geochemical and Isotopic Methods

Following the classification of Bayon et al. (2002), trace elements in marine sediments can be partitioned into five distinct fractions. Elements derived from seawater can be (1) adsorbed onto mineral surfaces (exchangeable fraction), (2) associated with carbonates, or (3) scavenged by iron and manganese oxides. The remaining trace metals in any sediment sample can be considered either (4) to be bound to organic compounds or (5) to belong to the detrital fraction.

The mechanism by which metals and other chemical species are bound onto solid matter (soils and sediments) may exert an important control on their geochemical behaviour. Several sequential extraction procedures have been developed for partitioning solid-phase metals, and they follow two main approaches, which differ mainly in their complexity. The simpler method involves separating a labile fraction from a residual fraction (Elderfield and Sholkovitz 1987; Snape et al. 2004), whereas the more complex approach involves using various reagents for the sequential removal of adsorbed elements, followed by carbonates, phosphates and Fe–Mn oxides (Das et al. 1995; Hall et al. 1996; Usero et al. 1998). Although the carbonate phase is typically removed from the bulk sediment in most of these methods, other authigenic fractions such as Fe–Mn oxides are usually retained (Négrel et al. 2000a; Freydier et al. 2001).

Leaching of sediment with cold HCl, which separates a labile fraction from a residue, is one of the most widely used reagents to isolate the non-residual phase of a variety of solids (Duinker et al. 1974; Banner et al. 1988; Négrel et al. 2000a; Freydier et al. 2001; Bayon et al. 2002; Snape et al. 2004). This reagent releases all the non-residual trace elements; i.e., those associated with hydrous Fe–Mn oxides (Kitano et al. 1981; Hall et al. 1996; Freydier et al. 2001; Yokoo et al. 2004), those adsorbed on clays (Bros et al. 1992; Clauer et al. 1993; Schaltegger et al. 1994), and those occurring in carbonates and sulfides in the sediment load, as well as in natural organic matter (Banner et al. 1988; Hall et al. 1996; Freydier et al. 2001; Worash and Valera 2002; Fanton et al. 2002). Fiszman et al. (1984) examined seven sediment samples from Sepetiba Bay, Brazil, and they concluded that dilute 0.1 M HCl was most closely associated with the summed concentrations liberated by three steps in a sequential extraction procedure: (1) amorphous oxides and carbonates (0.1 M hydroxylamine hydrochloride + 0.01 M HNO_3); (2) organic matter (30% H_2O_2); and (3) resistant crystalline Fe hydroxides (sodium citrate + sodium dithionite). Similar results were evidenced by Sutherland (2002) on more than 30 soil samples and demonstrating moreover that a single dilute HCl (0.5 N) leach approach minimally affected the crystal lattice.

Concerning the separation of a labile fraction from a residual one, considerable work has been done using hydrochloric acid with variable concentrations, (e.g., from 0.1 up to 12 M HCl). To assess extraction efficiency for a range of sediment types, four marine sediments were analyzed in detail by Snape et al. (2004). Using a 1 M HCl extraction, they concluded that no statistically significant differences can be evidenced between a 0.5 and 4 h HCl extraction, both allow the equilibrium dissolution of labile elements but do not favor the extraction of natural geogenic elements. Considering the different studies, involving a large range of sediment types in different marine or continental environments, it is therefore likely that minerals like feldspar and clays (illite, kaolinite, smectite, vermicullite) were not decomposed by HCl leaching with concentration from 0.2 to 1 M HCl, either on loess (Yokoo et al. 2004), on recent marine sediments (Haese et al. 1997; Ciaralli et al. 1998; Eisenhauer et al. 1999; Freydier et al. 2001), on carbonate-poor marine sediments (Emerson and Young 1995), on major marine sediment types (Van Valin and Morse 1982). The behavior of REE and Sm–Nd isotopes have also largely been studied with HCl as extractant. Study of the Nd isotope composition of eastern Mediterranean sediments indicate that the 1 M HCl residual and leachable fractions are adequate to represent the lithogenic, e.g., the silicate residue, and authigenic-biogenic fractions of the sediment, e.g., carbonates, organic matter, and Fe and Mn oxyhydroxides, as demonstrated by Freydier et al. (2001). Leaching of clay-rich rocks (Francevillian sedimentary series in Gabon, Cambrian claystone in Estonia, Cambrian shales of northwestern Morocco) in cold l N HC1 separates soluble-exchangeable Sm and Nd from amounts of these elements fixed in the crystallographic sites, without opening the lattice of the sediment (Bros et al. 1992; Clauer et al. 1993; Schaltegger et al. 1994). This has also been demonstrated on modern and late Quaternary sediment (Innocent et al. 1997; Fagel et al. 2002) and Upper Ordovician carbonates (Iowa Formation, North America; Fanton et al. 2002). On suspended matter collected by traps in the Sargasso Sea, Jeandel et al. (1995) demonstrated that leaching with 0.6 N HCl at 60°C for 20 h dissolved Nd not bound in the silicate phases, i.e., without opening the lattices or dissolving silicate minerals. Tachikawa et al. (1999a) and Tachikawa et al. (1999b) presented $\varepsilon Nd_{(0)}$ distributions of trapped sediment samples subjected to chemical leachings (0.6 N HCl or 25% acetic acid). The labile (i.e., the acid soluble) fractions $\varepsilon Nd_{(0)}$ were systematically closer to the seawater values at all depths at all sites, reflecting no extraction of geogenic elements.

Therefore, following these studies, we assume that the HCl digestion does not further disturb the clay-mineral lattice as well as partially dissolving silicates, and we consider the acid-extractable matter (hereafter referred to as AEM) as representing the elements bound onto Fe–Mn oxides, adsorbed on clays, and occurring in carbonates and sulfides as well as in natural organic matter in the sediment load.

Around 1 g of sediment was collected with an electric drill (Casanova et al. in press), following which representative aliquots were leached with cold 0.2 N HCl to separate a labile fraction from a residue. For the HCl extractions, solutions were prepared from an extra-pure quality grade concentrated HCl and deionized water. Teflon containers used for the extractions were cleaned in hot aqua regia and soaked and triple-rinsed in deionized water of resistivity < 18 MΩ cm. All extractions used 300 mg of sediment to 20 ml HCl solution in covered Teflon beakers, and an ultrasound treatment was performed at room temperature in an ultrasonic cleaning bath containing distilled water. Each sample was sonicated at room temperature, and the duration for the ultrasound–acid extraction was 30 minutes. After sonication and usual checks that the HCl had completely reacted with the sediment, the remaining solid residue was separated by centrifugation. The quantity of AEM representing the labile fraction was determined for each sample by the difference in weight between the dried sediment before and after acid extraction, and expressed as a percentage of the total matter content (Négrel et al. 2000a; Fanton et al. 2002). The error in the AEM determination is approximately $\pm$ 3%. The HCl solution (e.g., the AEM) was evaporated, the residual product was weighed, and aliquots were analyzed for Mn and REE contents and for Nd isotope composition.

The concentrations of Mn and REE in the AEM were determined by ICP-MS (VG Plasma Quad 2plus spectrometer at the joint BGRM-INSU-LPS Laboratory) and were expressed in µg per gram of matter (i.e., the residual product of the acid extraction). The analytical procedure for the REE determination (see Négrel et al. 2000a and Négrel et al. 2000b) used ^{139}La, ^{140}Ce, ^{141}Pr, ^{146}Nd, ^{147}Sm, ^{151}Eu, ^{157}Gd, ^{159}Tb, ^{163}Dy,

^{165}Ho, ^{167}Er, ^{169}Tm, ^{172}Yb, and ^{175}Lu REE isotopes to minimize the effects of interferences. Oxide and hydroxide interferences were corrected after analysis of pure solutions of Ba, Ce, Pr, Nd, Sm, Eu, Gd, and Tb. Instrumental drift was monitored and corrected using ^{115}In and ^{187}Re, where both internal standards were used according to an interpolation procedure. Calibration was performed using a SPEX standard solution, and a blank correction was applied to all samples and standard solutions; precision of the REE measurements is better than 5%.

The analytical techniques used for determination of Nd isotopes have been described elsewhere (Négrel et al. 2000b). The Nd isotopic compositions of the samples were determined after separation of Nd using classical cation exchange followed by HDEHP reverse chromatography with a total procedural blank less than 100 pg. The ^{143}Nd/^{144}Nd isotopic ratios were measured using a Finnigan MAT 262 multiple-collector mass spectrometer with samples loaded on double Re filaments; these were normalized to ^{146}Nd/^{144}Nd = 0.7219. Repeated measurements of the La Jolla international standard during the period of analysis yielded a mean ^{143}Nd/^{144}Nd of 0.511826 ± 0.000011 (2σ, n = 33). Usual in-run precisions of generally better than ± 0.00002 were obtained on ^{143}Nd/^{144}Nd ratios. The ^{143}Nd/^{144}Nd ratios are expressed as $\varepsilon Nd_{(0)}$, which represents the deviation in parts per 10^4 (ε units) from ^{143}Nd/^{144}Nd in a chondritic reservoir with a present-day CHUR value of 0.512638 (DePaolo and Wasserburg 1976) and as $\varepsilon Nd_{(t)}$, calculated following Equation 1:

$$10^4 \times \left[\left(^{143}\mathrm{Nd}/^{144}\mathrm{Nd}^{(t)}{}_{(\mathrm{sample})} - {}^{143}\mathrm{Nd}/^{144}\mathrm{Nd}^{(t)}{}_{(\mathrm{CHUR})}\right)/{}^{143}\mathrm{Nd}/^{144}\mathrm{Nd}^{(t)}{}_{(\mathrm{CHUR})}\right] \quad (1)$$

which represents the deviation in parts per 10^4 from ^{143}Nd/^{144}Nd in a chondritic reservoir with a Middle Jurassic CHUR value (Stille et al. 1996). ^{143}Nd/^{144}Nd$^{(t)}{}_{(\mathrm{sample})}$ was calculated according to Equation 2 (Faure 1986):

$$\left(^{143}\mathrm{Nd}/^{144}\mathrm{Nd}\right)_p = \left(^{143}\mathrm{Nd}/^{144}\mathrm{Nd}\right)_i + \left(^{147}\mathrm{Sm}/^{144}\mathrm{Nd}\right)_p\left(e\lambda^t - 1\right) \quad (2)$$

where the subscripts p and i refer to present-day and initial ratios and the superscript λ and t are the decay constant (6.5×10^{-12} y^{-1}) and time (y) since the formation of the system. The well-constrained ages for the sedimentary deposits (Jurassic) result in a robust correction for the ^{147}Sm decay influence. The test of a Jurassic age correction using Equation 2 induces a slight change in the ^{143}Nd /^{144}Nd ratio, ca 0.000083–0.000278 with a mean value of around 0.000126 and a standard deviation of around 0.000044.

RESULTS

The results of the Mn and REE data and the neodymium isotope compositions (with in-run precisions on the ^{143}Nd /^{144}Nd and on the $\varepsilon Nd_{(0)}$) from the HTM102 and EST106 cores are given in Table 1 and are illustrated in Figures 2 and 3.

The calcium carbonate distribution (Fig. 2) is asymmetric along the sedimentary profile, with higher carbonate contents at the top, at the bottom, and in the middle (e.g., $CaCO_3$ > 80% in the Tithonian, Late Bathonian, and Middle to Late Oxfordian), and a major decrease in $CaCO_3$ (20–40%) during the Kimmeridgian and Callovian–Early Oxfordian clay–marl layers (Casanova et al. in press).

The concentrations of individual REEs and total REEs (ΣREE) vary over several orders of magnitude in the AEM from the sedimentary column (Figs. 2, 3). Neodymium (Nd) concentrations reflect the variation in those of the individual REEs (Fig. 2), ranging from high values in the lower and upper parts of the sedimentary column (e.g., Late Callovian–Early Oxfordian and Late Kimmeridgian) to very low values in the intermediate part (e.g., Middle and Late Oxfordian). The variations in the AEM Nd curve are thus the mirror image of the carbonate curve (r^2 = −0.62), with low values corresponding to high carbonate content and vice versa. This is also the case for the ΣREE concentrations, which range from less than 1 μg g^{-1} in the Middle and Late Oxfordian layers up to 100 μg g^{-1} in the Late Callovian–Early Oxfordian and Late Kimmeridgian (Fig. 3). All the REEs measured along the sedimentary column show strong positive interelemental relationships (r^2 > 0.9), indicating their consistent nature and behavior. The ^{147}Sm/^{144}Nd ratios in the AEM range from 0.084 to 0.283 with a mean value of 0.127 and a standard deviation of 0.040. The ^{147}Sm/^{144}Nd ratios reported along the sedimentary column fluctuate largely in the Middle–Late Oxfordian in conjunction with the lowest Nd and Sm contents.

The AEM Mn contents along the sedimentary column again display an impressive mirror image of the carbonate curve (Figs. 2, 3), with high Mn being associated with the lower $CaCO_3$ and vice versa (Casanova et al. in press). Values in excess of 100 μg g^{-1} Mn were recorded in the lower part of the core before a major Mn decrease in the Middle to Late Oxfordian, with values descending to 6 μg g^{-1}. The Mn content then increases in the upper part of the Late Oxfordian, corresponding to an increase in the ΣREE, Nd, and Sm contents and a decrease in the $CaCO_3$ contents.

The Nd isotope composition in AEM from the sedimentary column shows fluctuations from ^{143}Nd/^{144}Nd ratios of less than 0.5121 up to ratios of 0.51235. Plotted as $\varepsilon Nd_{(0)}$ (Fig. 2, uncertainties on the ε are lower than the label size), it ranges from −11.84 ± 0.12 in the Late Callovian to −6.87 ± 1/−6.59 ± 0.24 in the Late Oxfordian (Table 1; Fig. 2). The Nd isotopes vary only slightly in the lower and upper parts of the sedimentary record, displaying $\varepsilon Nd_{(0)}$ values between −11.84 ± 0.12 and −10.57 ± 0.08 in the lower part of the sedimentary column (e.g., Early Callovian–Early Oxfordian) and in the upper part (Early Kimmeridgian–Tithonian). Two major peaks in the $\varepsilon Nd_{(0)}$ values of the AEM are seen in the middle and upper parts of the Late Oxfordian with values reaching −6.87 ± 1/−6.59 ± 0.24. Moving upwards in the column from these two levels, we see a lower $\varepsilon Nd_{(0)}$ values, around −10. On the basis of the analysis of various materials from different paleo-environments ranging from epicontinental (phosphatic fish remains, glauconites, and belemnites) to deep oceanic basins, the $\varepsilon Nd_{(0)}$ of the Tethys seawater during Oxfordian times ranged between −6.5 and −9 (Grandjean et al. 1987; Stille and Fischer 1990 and references therein; Stille et al. 1996). Our data generally agree with this range. The $\varepsilon Nd_{(0)}$ in our sedimentary column varies over a wide range of Nd concentrations but shows no direct link such as a linear relationship.

Some typical REE concentrations in the AEM are presented as normalized upper continental crust (UCC; Taylor and McLennan 1985) patterns in Figure 3. Among the different parameters that can be used to characterise the REE patterns, we focus here on different fractionation ratios (Table 2); i.e., normalized La/Yb, Pr/Yb, Er/Nd, and Dy/Yb ratios represented by $(La/Yb)_N$, $(Pr/Yb)_N$, $(Er/Nd)_N$, and $(Dy/Yb)_N$. The $(REE1/REE2)_N$ ratios are defined by the ratio $REE1_{sample}/REE2_{sample}$ to the ratio $REE1_{UCC}/REE2_{UCC}$, where UCC refers to the upper continental crust data from Taylor and McLennan (1985). Because the main source of REEs in the ocean is continental weathering and transport via rivers and estuaries, the resultant REE signature of the materials entering the oceanic cycle is a composite of the continental crust (de Baar et al. 1985; McLennan 1989). Therefore, because the REE concentrations of most shales and deep-sea sediments show similarly invariant patterns representative of typical average upper continental crust (c.f. McLennan 1989), we normalized our REE results to the UCC. In addition, because La can be variable and thus commonly higher than suggested by the

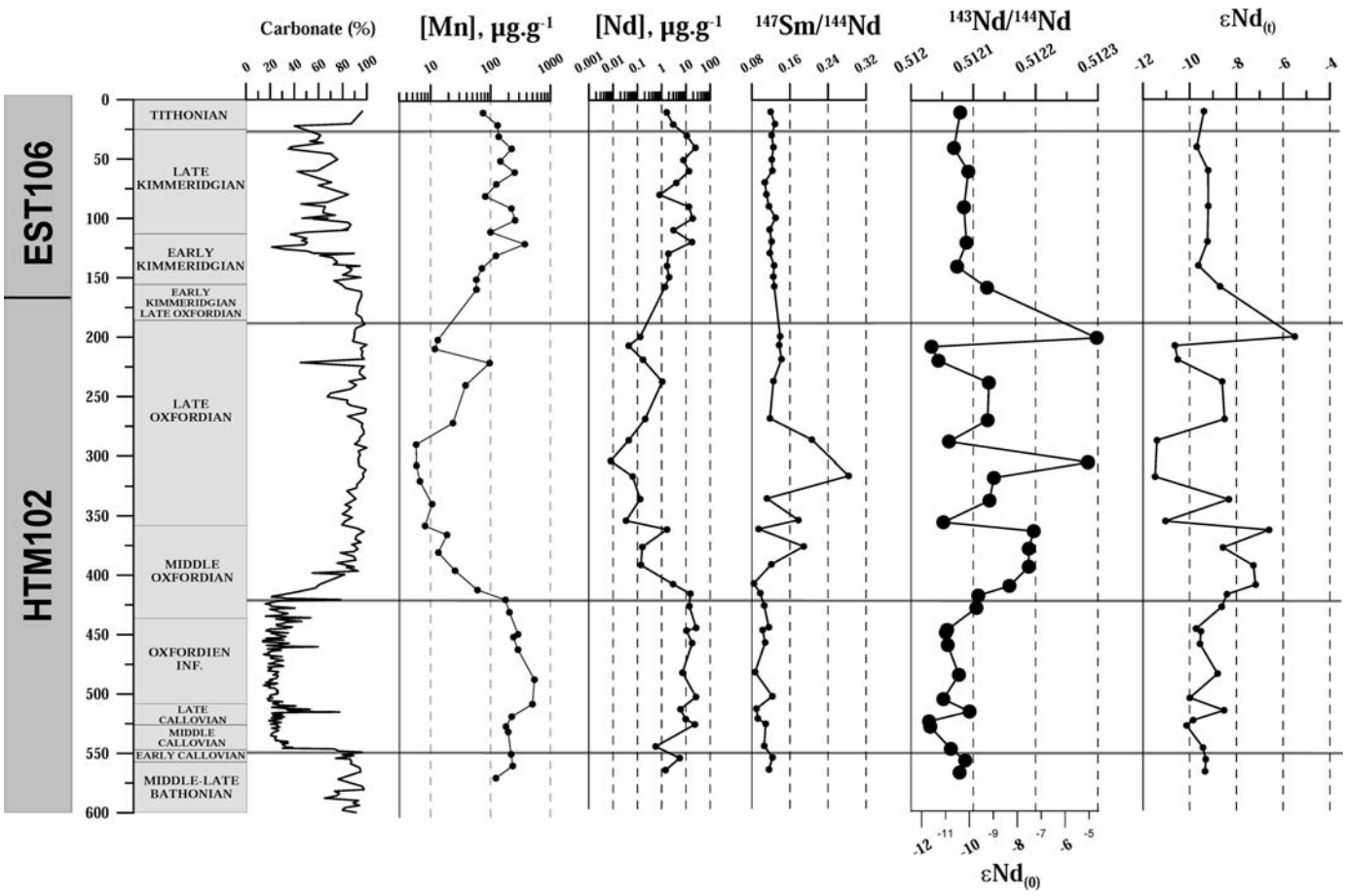

FIG. 2.—Downcore variations of carbonate content (in %), Nd contents (in µg g^{-1}), Nd isotopes ($^{143}Nd/^{144}Nd$, $\varepsilon Nd_{(0)}$ and $\varepsilon Nd_{(t)}$), and Mn contents (in µg g^{-1}) in cores HTM102 and EST106 of Middle to Late Bathonian to Tithonian sediments. It is worth noting that the uncertainties on the $\varepsilon Nd_{(0)}$ (using the in-run precision) are lower than the label size.

neighboring REE (Négrel et al. 2000b; Shields and Stille 2001), we used both La/Yb and Pr/Yb normalized ratios.

The REE in the AEM exhibited relatively uniform patterns that illustrate the main features of the lithologies of the sedimentary column. In the Callovian–Oxfordian clay layer, the REE patterns display enrichment in light REE (LREE) relative to heavy REE (HREE) with a $(La/Yb)_N$ ratio in the 1.9–2.5 range, in agreement with the $(Er/Nd)_N$ ratio, which ranges from 2.1 to 2.4. These patterns are also characterized by a strong decrease in REE abundance from Gd to Lu {$(Dy/Yb)_N = 1.9$}. Another feature of these patterns is a slight enrichment in middle REE (MREE; e.g., Eu, Gd, Tb, and Dy) compared to LREE and HREE, inducing higher UCC-normalized ratios for MREE than for LREE and HREE. In the Middle to Late Oxfordian carbonate-rich layer, the REE exhibit relatively similar patterns. The $(La/Yb)_N$ ratio decreases upwards from 2.3 (363.2 m depth) to 0.69 (200.41 m depth), but the $(Pr/Yb)_N$ ratio, which is close to 1 at 363.20 m depth, is around 0.3–0.4 in the upper part of the Oxfordian. This reflects a marked enrichment of the heaviest HREE upwards, as confirmed by the increase of the $(Er/Nd)_N$ ratio from 1.1 to 3.3 and by the decrease of the $(Dy/Yb)_N$ ratio. Lastly, the normalized REE patterns in the Early and Late Kimmeridgian AEM have a $(La/Yb)_N$ ratio in the range 1.0–1.8, which indicates a slight enrichment in LREE compared to HREE and is in agreement with the $(Er/Nd)_N$ ratio, which is around 0.9. However, these patterns are not flat, but are largely enriched in MREE with higher UCC-normalized ratios for MREE compared to LREE and HREE.

All the patterns have a negative Ce anomaly (e.g., $Ce/Ce^* = 2Ce_N/[La_N + Pr_N]$), with Ce/Ce^* ranging from 0.18 to 0.3 in the Middle to Late Oxfordian carbonate layers, but only 0.7 to 0.8 in the Callovian–Oxfordian clay layers and 0.9 to 1.0 in the Early and Late Kimmeridgian layers. As stated by Shields and Stille (2001), there is a possibility that the Ce anomaly in sediments may be exaggerated by the anomalous La_N enrichment relative to Pr_N. This effect can be tested by calculating the praseodymium values (Pr/Pr^*) according to $Pr_N/(0.5Ce_N + 0.5Nd_N)$. Following Shields and Stille (2001), the existence of a true Ce anomaly should lead to $(Pr/Pr^*) > 1$. Except for one sample (located at 219.7 m depth), the (Pr/Pr^*) values ranged from 1.05 to 1.40, the highest values being observed in the lower and upper parts of the sedimentary column, and therefore reflecting real Ce anomalies.

DISCUSSION

Behavior of Carbonate, Manganese, and REE

Since the pioneering work of Piper (1974), it is generally believed that marine carbonate phases are low in REEs in comparison with detrital clays and heavy minerals. Therefore, dilution of a terrigenous component by biogenic calcite can be an important factor controlling ΣREE abundance, as Bellanca et al. (1997) demonstrated through a strong negative correlation between ΣREE and CaO in a stratigraphic Albian to Cenomanian succession. Our data suggest an identical process when comparing the fluctuations of Nd and ΣREE in the AEM and carbonate

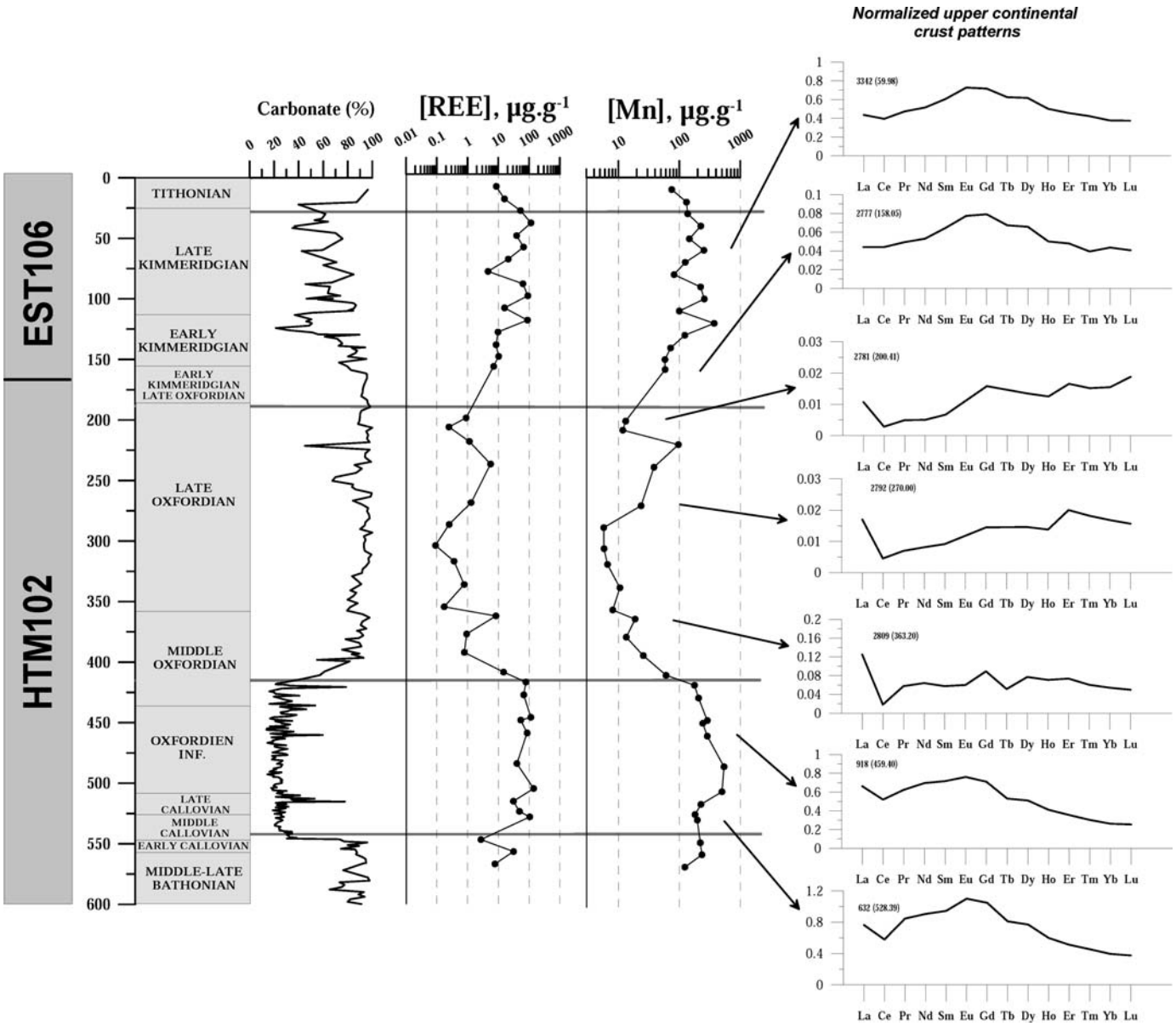

FIG. 3.—Downcore variations of carbonate content (in %), REE contents (in µg g^{-1}), and Mn contents (in µg g^{-1}) in cores HTM102 and EST106. Comparison of representative REE patterns (normalized upper continental crust; Taylor and McLennan 1985) along the sedimentary column.

contents, as shown in Figures 2 and 3. Thus, considering the entire sedimentary column, the large positive correlation between the ΣREE and Mn ($r > 0.8$) in the AEM suggest that Mn-bearing phases (e.g., oxyhydroxides and aluminosilicate lattices) probably have an important influence on REE control. The impact of the HCl leaching on the silicate, e.g., severe leaching inducing removal of elements from the mineral structure, can be discarded by looking at the fluctuations of the Sr isotopes on the sedimentary column. Casanova et al. (1999) showed that the $^{87}Sr/^{86}Sr$ ratios of the leaching are mostly in agreement with that of the contemporaneous Jurassic seawater, even in the clay-rich sections (Late Callovian–Early Oxfordian–Kimmeridgian).

It is worth noting that Mn oxyhydroxides are ubiquitous in oxic to suboxic environments (Morford and Emerson 1999). They may occur as discrete grains, particles (commonly colloidal), flocs precipitated from bottom seawater and/or pore water prior to diagenesis (Vance and Burton 1999; Rutberg et al. 2000; Bayon et al. 2004), or as coatings on other solids (e.g., on foraminifera, Palmer and Elderfield 1986. Coatings on siliciclastic particles derived from continental weathering as river-sediment input can also be a source of Mn–Fe oxyhydroxides (Piper 1974; de Baar et al. 1985; Wang et al. 1986; Banakar et al. 1998; Fallon et al. 2002) and reflect the terrigenous influence. Due to their large surface areas, the Mn–Fe oxyhydroxides are very effective scavengers and therefore exert an important control on the concentration and migration of elements such as REEs (Elderfield et al. 1981; Bau 1999; Ohta and Kawabe 2001; Bayon et al. 2002). For example, Koschinsky et al. (2003) evidenced that manganese and Fe oxides and oxyhydroxides play a much stronger role in scavenging dissolved trace elements, compared to other mineral phases present in deep-sea environment such as clay minerals and detrital aluminosilicates. On the other hand, REEs in marine carbonates are derived mainly from bottom seawater or indirectly from pore water that is near the seawater–sediment interface and interconnected with bottom seawater (Elderfield et al. 1981; Elderfield and Greaves 1982;

TABLE 2.—*Selected parameters that characterize the typical REE normalized patterns illustrated in Figure 3.*

Samples	Depth (m)	La/Yb_N	Pr/Yb_N	Er/Nd_N	Dy/Yb_N	Ce/Ce*
EST106						
3330	10.08	1.14	1.08	1.12	1.62	0.83
3334	20.42	0.97	0.94	1.20	1.53	0.83
3338	29.95	1.14	1.23	0.92	1.61	0.80
1298	40.08	1.31	1.56	0.78	2.00	0.91
3341	50.55	1.02	1.05	1.03	1.52	0.80
3342	59.98	1.16	1.25	0.89	1.64	0.88
3345	69.88	1.73	1.51	0.84	1.63	0.72
3348	80.00	1.73	1.25	1.14	1.69	0.70
3349	90.13	1.57	1.66	0.71	1.71	0.83
3351	100.03	1.26	1.47	0.79	1.85	0.93
3356	109.96	1.18	1.08	1.06	1.42	0.75
1472	120.03	1.36	1.46	0.81	1.84	0.91
3359	129.83	1.30	1.27	0.95	1.62	0.81
3360	140.30	1.12	1.18	0.88	1.54	0.91
3364	149.84	1.12	1.26	0.89	1.50	0.92
HTM 102						
HTM 2777	158.05	1.01	1.13	0.90	1.51	0.96
HTM 2781	200.41	0.69	0.32	3.30	0.87	0.32
HTM 2783	207.90	—	—	3.34	—	0.42
HTM 2785	219.75	1.13	0.58	2.66	1.00	0.59
HTM 2788	238.35	0.95	0.70	1.71	1.26	0.52
HTM 2792	270.00	1.01	0.41	2.48	0.87	0.33
HTM 2796	288.01	—	—	3.60	—	0.29
HTM 2799	305.25	—	—	—	—	—
HTM 2801	318.24	0.39	0.23	2.65	0.73	0.23
HTM 2805	337.37	1.22	0.47	2.17	1.02	0.20
HTM2845	355.68	—	—	—	—	—
HTM 2809	363.20	2.30	1.06	1.15	1.41	0.18
HTM 2813	378.03	0.84	0.33	2.47	0.76	0.15
HTM 2816	393.19	1.61	0.64	1.94	1.22	0.27
HTM616	409.41	3.56	1.88	0.73	1.78	0.34
HTM80619	417.56	3.04	2.40	0.55	1.85	0.63
HTM621	428.08	2.35	2.11	0.61	1.87	0.68
HTM856	446.56	2.25	2.51	0.50	2.00	0.79
HTM 80665	448.84	2.97	2.34	0.50	1.89	0.67
HTM 918	459.40	2.52	2.37	0.51	1.94	0.80
HTM 1017	484.53	3.30	2.45	0.61	1.99	0.76
HTM630	505.08	1.81	1.83	0.66	1.83	0.92
HTM598	515.54	3.81	2.42	0.64	1.98	0.49
HTM 1177	523.86	3.59	2.59	0.52	1.95	0.57
HTM632	528.39	1.94	2.14	0.57	1.95	0.73
HTM636	547.08	1.39	1.14	0.95	1.44	0.58
HTM 2822	556.90	1.18	0.90	1.13	1.30	0.70
HTM 2825	567.10	1.20	0.93	1.32	1.57	0.65

The La/Yb, Pr/Yb, Er/Nd and Dy/Yb normalized ratios are represented by $(La/Yb)_N$, $(Pr/Yb)_N$, $(Er/Nd)_N$, $(Dy/Yb)_N$. The $(REE1/REE2)_N$ ratios are defined by the ratio $REE1_{sample}/REE2_{sample}$ to the ratio $REE1_{UCC}/REE2_{UCC}$, where UCC refers to upper continental crust (Taylor and McLennan 1985).

Wang et al. 1986); in the case of a large presence of planktonic foraminifera in the sediment, the REE and Nd isotope composition of contemporary seawater from which the foraminiferal calcite was precipitated is recorded (Vance and Burton 1999), rather than that of pore waters or bottom waters. REE abundance in seawater is low and, therefore, incorporation of REE in carbonates leads to lower concentrations than in Mn oxyhydroxides (Wang et al. 1986; Bellanca et al. 1997; Webb and Kamber 2000; Worash and Valera 2002).

The REE patterns, partly illustrated in Figure 3, can provide reliable information on the processes controlling REEs and their origin like the effect of dilution by the carbonate dissolution, with very low REE content, cannot be the main processes in generating the observed relationships between Mn, Nd, and ΣREE and carbonate contents in the AEM. Considering the sedimentary column, it is worth noting similar Mn, Nd, and REE contents in the Callovian–Oxfordian and Kimmeridgian whereas the carbonate content differs largely (around 20% in the Callovian–Oxfordian; between 40 and 80% in the Kimmeridgian). The REE in the carbonate-rich section, bound onto carbonate and Mn oxyhydroxide are low, due to the low REE content in the carbonate fraction, which may reflect the lower scavenging capacity of carbonate, with regard to REE, compared to Mn oxyhydroxides. This precludes a large influence of carbonate dilution on the REE patterns.

Typical "bell-shaped" REE patterns are observed in the lower and upper parts of the sedimentary column (e.g., Late Callovian–Early Oxfordian and Kimmeridgian), which agree with a Mn-oxyhydroxide control. Fe–Mn coatings on siliciclastic particles and on solid matter in river systems have been recognized as efficient carriers of REE with an MREE-enriched pattern (e.g., the "bell-shaped" REE pattern; Granjean-Lecuyer et al. 1993; Tricca et al. 1999; Négrel et al. 2000a; Négrel et al. 2000c; Bayon et al. 2004) corresponding to a high level of manganese in all of the sedimentary record. All authors related such enrichment to Mn oxyhydroxides in the form of coatings on siliciclastic particles (Bayon et al. 2004). Such patterns in the sediments should therefore be related to a period of higher river runoff with a greater detrital input. This is also

suspected in the upper part of the sedimentary column, even if the carbonate shoals of the Oxfordian platform acted as a protection against continental input. This agrees with the recent work of Picard et al. (2002), who demonstrated that vertebrate teeth from the siliciclastic sediments of the Anglo–Paris Basin display normalized REE patterns reflecting a dominant influence of the continental source from which the REEs were derived. It is worth noting that the REE patterns during the Late Bathonian and earliest Tithonian, when the carbonate content was high and the Mn content showed slight increases or decreases, also display an MREE enrichment and a "bell-shaped" pattern in the AEM.

However, it is now well accepted that the distribution of manganese in marine environments could also be due to the presence of micronodular Mn (Tachikawa et al. 1999b) with REE patterns similar to that of seawater. Once deposited, the Mn phases are highly susceptible to dissolution, thus supporting an upward diffusion of Mn (II) ions, below a few tens of centimeters of the sediment with interface, and reprecipitation of Mn (IV) as oxides. Such a process near the sediment–water interface (Banakar et al. 1998; Morford and Emerson 1999) generally retains the REE pattern of seawater or pore water. In a recent study Haley et al. (2004) presented a hypothetical model for distribution of REEs in the water column and pore water. The results of the model predicted a large dynamic range with various REE patterns in the pore water. The REE patterns with negative Ce anomalies and slight to significant HREE enrichment (e.g., similar to that of seawater; Elderfield and Greaves 1982) are observed only in the middle part of the sedimentary column in the Middle to Late Oxfordian (Fig. 3). Because marine carbonate phases record the local seawater REE signature (Elderfield et al. 1981; Whittaker and Kyser 1993) and marine precipitates display HREE enrichment (Elderfield and Greaves 1982; Wang et al. 1986), it could be considered that REE in the Oxfordian platform are mainly linked to carbonate precipitation plus the fraction linked with the Mn oxyhydroxides. As illustrated by the Mn profile, which reflects low Mn oxyhydroxide contents, the carbonate shoals of the Oxfordian platform were biochemically deposited from seawater in basin domains that were relatively well protected from detrital influence. They contain REE reflecting the composition of the overlying water column, recorded by carbonate and Mn oxyhydroxides formed in the marine environment, as demonstrated by Webb and Kamber (2000) on ancient reefal limestones that may provide reliable seawater REE proxies.

Therefore, we can postulate that a large part of the REE in the sediment was associated with authigenic components (e.g., the Mn oxyhydroxides and the carbonate), although we still have the unresolved question as to the origin of these authigenic components: hydrogenously formed within the seawater column and/or through early diagenetic processes in the sediment, or hydrogenously formed on the continent. As stated above, Fe–Mn coatings on siliciclastic particles could be one of the most effective sources, in addition to reflecting a continental input to the platform. This terrigenous origin for the labile fraction in the sedimentary column may preserve a record of the oxyhydroxides generated on the continent through weathering processes (Fallon et al. 2002) and probably reflects the REE distribution within the exposed continental crust. The REE trends in the AEM are likely to reflect the Mn oxyhydroxides, but without any constraint on their origin because the investigation of REE patterns alone does not allow inference of the ultimate process leading to the observed patterns. This will be further constrained by the neodymium isotope results.

Nd Isotopes as Independent Fingerprints of REE Sources

Several authors have established that major interoceanic differences exist in Nd isotopes, which enables the pathways and mixing of water masses to be traced at the ocean basin scale (Amakawa et al. 2000; Frank 2002). Attempts to reconstruct the evolution of past Nd isotopes in global oceans suggest that these differences have existed throughout geological time (Stille et al. 1996; Frank et al. 1999; Frank 2002). Furthermore, correlation of Late Ordovician epicontinental marine carbonates of central North America using Nd isotope profiles demonstrates the potential of Nd isotope stratigraphy (Fanton et al. 2002). The possible effects of diagenetic processes on the REE and Nd-isotope signature can be discarded in the sedimentary record from the eastern Paris Basin. Diagenetic processes are divided into three steps: phreatic diagenesis; dolomitization within the marine- and fresh-water environments, mainly during the Middle to Late Oxfordian; and shallow burial diagenesis (Pellenard et al. 1999; Andra 2001). As demonstrated by Banner et al. (1988), the Nd values of marine limestones remain unchanged during episodes of extensive dolomitization, and the fluid/rock ratios required to alter the Nd values of the original limestone, the Fe–Mn coatings and the biogenic apatite are generally not encountered (Banner et al. 1988; Grandjean et al. 1988; Holmden et al. 1996). Because all the diagenetic processes along the sedimentary record from the east of the Paris Basin have been classified as being slight (Pellenard et al. 1999), we have assumed that none of the changes in the Nd isotope signatures are linked with diagenesis and that consequently the Nd isotopes reflect the signature of the Nd sources.

The Nd isotopes in the AEM have been compiled in $\varepsilon Nd_{(t)}$ evolution diagram (Fig. 4) that reflects the time variation of the different oceanic waters from the Pacific, the Atlantic, and the Tethys over the past 250 Ma (diagram from Stille et al. 1996, and references therein); the evolution of the continental crust is also illustrated. It should be noted that this diagram results from a databank that includes many sediment locations and water depths. The history of the Tethys seawater, decoupled from the Panthalassa seawater, began with a decrease of the Nd isotope signature, related mainly to the break up of Pangea. Continental runoff, with nonradiogenic Nd values, induced the evolution of the Tethys seawater between 180 and 90 Ma (Stille et al. 1996), with the lowest Nd values being reached in the Early Cretaceous.

Our data, plotted in Figure 4, focus on the decrease of the Nd isotope composition of the Tethys seawater. The $\varepsilon Nd_{(t)}$ in the AEM along the sedimentary column fluctuates between two extreme endmembers. Most of the data plot within the continental-crust field, this corresponding mainly to a neodymium source from the continent and/or emerged areas and with extensive exposure of the basement rocks to erosion. At the other extreme, the higher radiogenic Nd shifts in the AEM reflect larger inputs of neodymium with a typical Tethys seawater signature; these shifts, with the $\varepsilon Nd_{(t)}$ between -6.6 and -5.5, occurred during the Late Oxfordian (Fig. 2). Some intermediate radiogenic Nd shifts are also recognized in the Late Oxfordian (Fig. 2), with the $\varepsilon Nd_{(t)}$ around -8, but these never reach the Nd isotope composition of the Tethys seawater.

Within the studied interval, the seawater Nd budget was dominated mainly by continental sources. Since the work of Keto and Jacobsen (1987), it is generally accepted that the Nd isotope compositions of oceans throughout the Phanerozoic were dominated by river inputs. Among the process required to balance the oceanic Nd budget, Tachikawa et al. (1999b) suggested partial dissolution from atmospheric fallout (more than 20%) and/or other additional sources (e.g., dissolved–particulate Nd exchange). However, recently, Tachikawa et al. (2003) and Lacan and Jeandel (2005), studying the global Nd isotope composition and concentration distributions with a ten-box ocean model, estimated that eolian and riverine inputs are insufficient to account for the variations in Nd concentration and Nd isotope composition observed among the different oceanic basins. They suggest that continental margins could supply the missing Nd to the ocean. Therefore, it is obvious that weathering of rocks of different types will deliver Nd values with regionally distinctive isotopic compositions, in either a river basin (Allègre et al. 1996), a synorogenic foreland basin (Robinson et al. 2001), or an oceanic-basin setting (Amakawa et al. 2000). This is

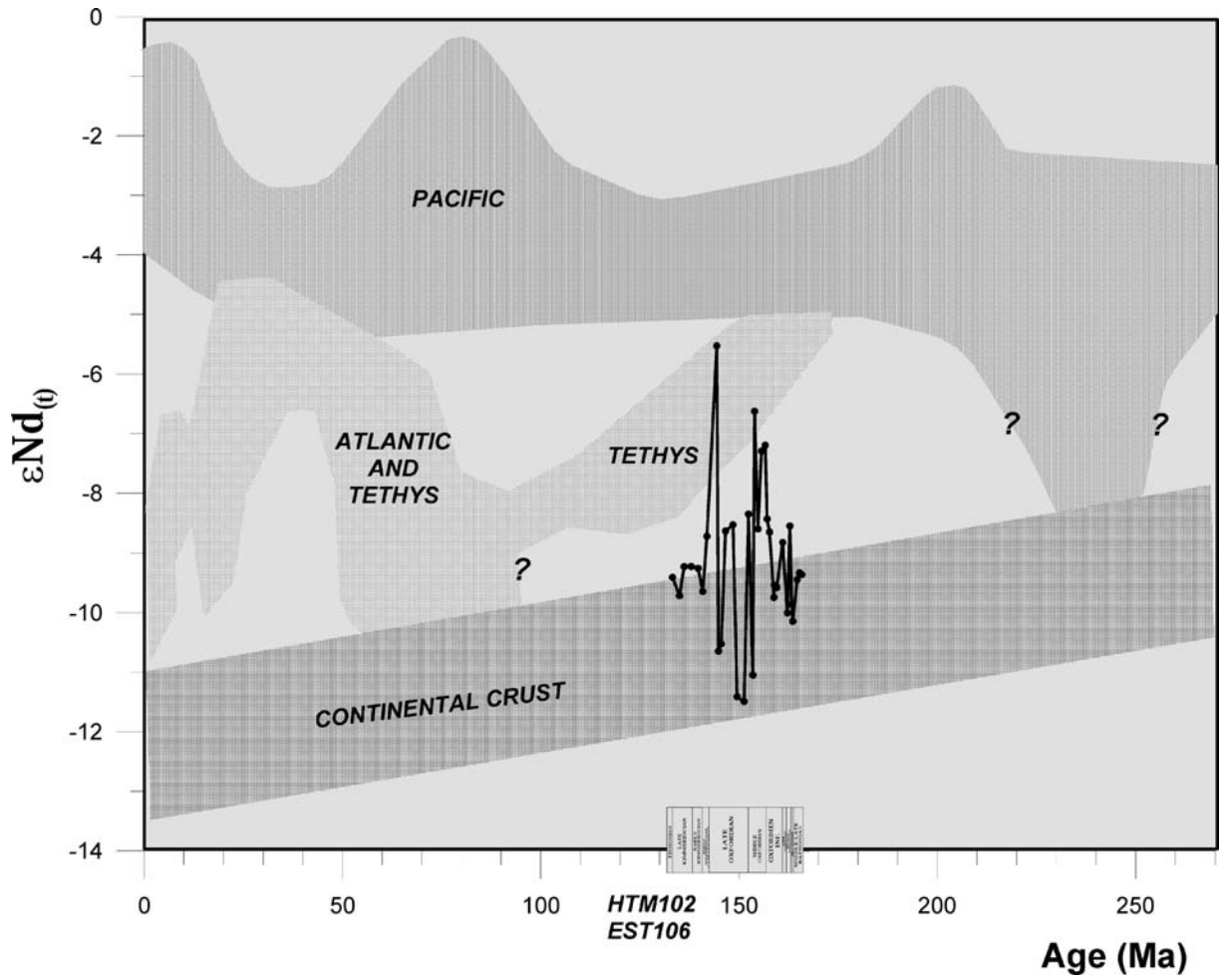

FIG. 4.—$\varepsilon Nd_{(t)}$ evolution diagram of Pacific Ocean, the Atlantic Ocean, and Tethys seawater over the past 250 Ma (from Stille et al. 1996, and references therein). The curve represents the $\varepsilon Nd_{(t)}$ evolution along cores HTM102 and EST 106. The lithological log (Fig. 1) is also indicated.

illustrated by the rivers entering the Atlantic Ocean, influenced by old continental crust and displaying nonradiogenic Nd isotope compositions (Goldstein and Jacobsen 1987, 1988; Allègre et al. 1996). Most values observed in the sedimentary record are consistent with (a) those of the pre-Variscan crust (Michard et al. 1985; Liew and Hofmann 1988; Simien et al. 1999) and residual erosion products of the Variscan-crust granites of the Alps (Henry et al. 1997), and (b) those of the Variscan-crust granites and gneisses of the Massif Central (Downes and Duthou 1988; Pin and Duthou 1990) and the Vosges Mountains (Tricca et al. 1999; Aubert et al. 2001). We can conclude, therefore, that the nonradiogenic $\varepsilon Nd_{(t)}$ values in the AEM in the sedimentary record mainly reflect the average isotope composition of the various crustal segments that were exposed and eroded during this period. But it is not possible to relate $\varepsilon Nd_{(t)}$ variations to sea-level or tectonic variations using the Nd isotopic composition in the sedimentary record. However, because clay-size fractions may be transported far from their continental sources, it is difficult to constrain the source zone of their terrigenous component. Stille and Fischer (1990) demonstrated that the average isotopic composition of the continental source was relatively constant from the Middle Jurassic up to the Tertiary, although a decrease in the average continental-crust $\varepsilon Nd_{(t)}$ can be seen in Figure 4.

During the Late Bathonian, the $\varepsilon Nd_{(t)}$ of the labile fraction of the carbonate platform reflects the value of the continental crust. The Middle Callovian–Early Oxfordian consists of argillite, essentially comprising detrital illite–smectite clay (60%) with quartz and K-feldspar (Vieillard et al. 2004), and therefore the $\varepsilon Nd_{(t)}$ marks the signature of the continental crust (Figs. 2, 5). During the Middle Oxfordian, the progradational character of the deposits led to the development of a carbonate platform with a mixed terrigenous–carbonate system (Pellenard et al. 1999). This is again clearly reflected by the $\varepsilon Nd_{(t)}$, which evolves from typical "continental crust" values (i.e., around -12 to -10) to a roughly "Tethyian" value of ~ -8 to -6 (Figs. 2, 5). This evolution is accompanied by a decrease in the Mn content (Figs. 2, 3), whilst the Nd may have been controlled mainly by the marine carbonate plus the part controlled by the Mn oxyhydroxides as suggested by the typical REE pattern (Fig. 3). The variation of the $\varepsilon Nd_{(t)}$ from a continental to a "Tethian" value agrees well with the conclusions of Carpentier et al. (2004). They showed for the Oxfordian platform of Lorraine (eastern Paris Basin, a few tens of kilometers from HTM102 and EST106 boreholes) that it was opened to the southeast towards the Tethys but also to the north east to the Germanic Sea. The latest connection would probably have been responsible for the continental inputs.

The Late Oxfordian, although dominated by typical reefal facies, also included continental input. This is clearly evidenced by the $\varepsilon Nd_{(t)}$ that evolved between the two endmembers: the continental-crust and the Tethys-seawater signatures. Some terrigenous facies have been recognized in the Late Oxfordian (Pellenard et al. 1999; Andra 2001), where the $\varepsilon Nd_{(t)}$ reflects an increase in detrital input with values lower than -10.

Conversely, marine sedimentation with a typical Tethys-seawater signature (around −5) is also evidenced in the Late Oxfordian. The transition from the Late Oxfordian to the Early Kimmeridgian is marked by a low $\varepsilon Nd_{(t)}$ value, in agreement with a higher detrital flux as reflected by the clay content and mineralogy (Pellenard et al. 1999; Andra 2001). The $\varepsilon Nd_{(t)}$ values reach a typical continental-crust signature of around −10 to −9 during the Early Kimmeridgian, a value that remained invariant during the Late Kimmeridgian and reflects the new deeper marine system with clayey deposits. The Tithonian, comprising infralittoral to supralittoral carbonates, displays $\varepsilon Nd_{(t)}$ values in the continental-crust range, reflecting the detrital origin of Nd from continental weathering processes (Fig. 4).

To conclude, the $\varepsilon Nd_{(t)}$ of the labile fraction retains the isotopic signature of its source rocks (e.g., the continental crust) throughout all the continental-weathering and sediment-transport processes. Transgressions (e.g., Tethysian inputs to the platform) are recorded as positive Nd isotopes shifts in the carbonate deposits. Regressions and/or changes in the sedimentary system (e.g., connection with the Germanic Sea; Carpentier et al. 2004) are recorded as negative isotope shifts when the basement was once again exposed to weathering. As assumed by Fanton et al. (2002), and also evidenced in the sedimentary record from the eastern Paris Basin, the dissolvable phases (carbonate and Mn oxyhydroxides) in the carbonate platform appear to have recorded the Nd of seawater, whereas Fe–Mn coatings on detrital continental particles raise the Nd concentrations and lead to less radiogenic $\varepsilon Nd_{(t)}$.

CONCLUSIONS

By combining manganese and REE analysis data with Nd isotope data of the labile fraction in the Callovian–Oxfordian–Tithonian marine sediments of the Late Jurassic carbonate platform in the eastern part of the Paris Basin, our study comes to several conclusions concerning the origin and transport mechanisms of REE. The concentrations of manganese clearly mirror the carbonate content as well as that of individual and total REE (ΣREE) contents, which vary over several orders of magnitude in the sedimentary column. Considering the entire sedimentary column, the large positive correlation between the ΣREE and Mn ($r > 0.8$) in the AEM suggest that Mn-bearing phases (e.g., oxyhydroxides and aluminosilicate lattices) probably have an important influence on REE control.

The REE patterns are similar to those of seawater in the middle part of the sedimentary record, suggesting REE removal by marine carbonate, while bell-shaped REE patterns are observed above and below, reflecting continent-derived REE carried by Fe–Mn coatings on detrital particles. Therefore, we can postulate that a large part of the REE in the sediment is associated with a authigenic components (e.g., the Mn oxyhydroxides) but the origin of these authigenic components—hydrogenously formed within the seawater column and/or through early diagenetic processes in the sediment, or hydrogenously formed on the continent—remains unsolved.

The Nd isotopes in the AEM have been compiled in an $\varepsilon Nd_{(t)}$ evolution diagram that reflects the time variation of the different oceanic waters from the Pacific, the Atlantic, and the Tethys over the past 250 Ma. The nonradiogenic values ($\varepsilon Nd_{(t)}$ around −12, −10) strongly suggest that the predominant source of Nd on the platform is from the continental crust and that the Nd isotope composition of the riverine inputs are faithfully reflected in the labile fraction, whereas higher radiogenic Nd shifts reflect a larger input of neodymium with a typical Tethys-seawater signature.

ACKNOWLEDGMENTS

This work was financially supported by joint research programs from the Andra Scientific Division and the BRGM Research Division. The Callovian–Oxfordian clay–marl layer is the potential target of reconnaissance work carried out by Andra (*National Agency for Radioactive Waste Management*) in eastern France, the purpose of which is to design and build an underground research laboratory for studying the capability of these deposits for the storage of radioactive waste. The work benefited from the collaboration of C. Guerrot (TIMS team), and A. Cocherie (ICP-MS team), who provided the Nd isotope and trace-element and rare-earth-element analyses, respectively. We are grateful to P. Skipwith and R. Stead from the BRGM Translation Service for improving the English and to F. Simien, C. Lecuyer, and S.N. Ehrenberg for their critical reviews on an earlier version of this manuscript. We also thanks the two anonymous reviewers and Associate Editor Maria Mutti.

REFERENCES

Allègre, C.J., Dupre, B., Négrel, P., and Gaillardet, J., 1996, Sr–Nd–Pb isotopes systematics in Amazon and Congo River systems. Constraints about erosion processes: Chemical Geology, v. 131, p. 93–112.

Amakawa, H., Alibo, D.S., and Nozaki, Y., 2000, Nd isotopic and REE pattern in the surface waters of the eastern Indian Ocean and its adjacent seas: Geochimica et Cosmochimica Acta, v. 64, p. 1715–1727.

Andra, 2001, Référentiel géologique du site de Meuse/Haute-Marne, v. 1–4, Available upon request to Andra (www.andra.fr). Andra report ARP ADS 99-005, 487 p.

Aubert, D., Stille, P., and Probst, A., 2001, REE fractionation during granite weathering and removal by waters and suspended loads: Sr and Nd isotopic evidence: Geochimica et Cosmochimica Acta, v. 65, p. 387–406.

Banakar, V.K., Parthiban, G., Pattan, J.N., and Jauhari, P., 1998, Chemistry of surface sediment along a north–south transect across the equator in the Central Indian Basin: an assessment of biogenic and detrital influences on elemental burial on the seafloor: Chemical Geology, v. 147, p. 217–232.

Banner, J.L., Hanson, G.N., and Meyers, W.J., 1988, Rare earth element and Nd isotopic variations in regionally extensive dolomites from the Burlington–Keokuk Formation (Mississippian): implications for REE mobility during carbonate diagenesis: Journal of Sedimentology Petrology, v. 58, p. 415–432.

Bau, M., 1999, Scavenging of dissolved yttrium and rare earths by precipitating iron oxyhydroxide: experimental evidence for Ce oxidation, Y–Ho fractionation and lanthanide tetrad effect: Geochimica et Cosmochimica Acta, v. 63, p. 67–77.

Bayon, G., German, C.R., Boella, R.M., Milton, J.A., Taylor, R.N., and Nesbitt, R.W., 2002, An improved method for extracting marine sediment fractions and its application to Sr and Nd isotopic analysis: Chemical Geology, v. 187, p. 179–199.

Bayon, G., German, C.R., Burton, K.W., Nesbitt, R.W., and Rogers, N., 2004, Sedimentary Fe–Mn oxyhydroxides as paleoceanographic archives and the role of aeolian flux in regulating oceanic dissolved REE: Earth and Planetary Science Letters, v. 224, p. 477–492.

Bellanca, A., Masetti, D., and Nri, R., 1997, REE in limestone/marlstone couplets from the Albian–Cenomanian Cismon section (Venetian Region, northern Italy): assessing REE sensitivity to environmental changes: Chemical Geology, v. 141, p. 141–152.

BRGM, 1996, Geological Map of France, 1:1,000,000 scale, 6th edition: BRGM.

Bros, R., Stille, P., Gauthier-Lafaye, F., Weber, F., and Clauer, N., 1992, Sm–Nd isotopic dating of Proterozoic clay material: An example from the Francevillian sedimentary series, Gabon: Earth and Planetary Science Letters, v. 113, p. 207–218.

Carpentier, C., Lathuiliere, B., and Ferry, S., 2004, The Oxfordian platform of Lorraine: evidences for an opening toward the Germanic Sea: Comptes Rendus, Geosciences, v. 336, p. 59–66.

Casanova, J., Négrel, P., Aaranyossy, J.F., and Brulhet, J., 1999, Callovo–Oxfordian argillites (Meuse, France): Isotope Geochemistry (O, C, Sr): 3rd International Symposium on Applied Isotope Geochemistry, September 21–25, Orléans, France. 127–128.

Casanova, J., Négrel, P., and Brulhet, J., in press, Behaviour of nuclides and U-series disequilibrium in clayey sediments: application to the Late Jurassic record from the eastern Paris basin: Journal of Geochemical Exploration.

Ciaralli, L., Giordano, R., Lombardi, G., Baccaloni, E., Sepe, A., and Costantini, S., 1998, Antarctic Marine Sediments: Distribution of Elements and Textural Characters: Microchemical Journal, v. 59, p. 77–88.

Clauer, N., Chaudhuri, S., Kralik, M., and Bonnot-Courtois, C., 1993, Effects of experimental leaching on Rb–Sr and K–Ar isotopic systems and REE contents of diagenetic illite: Chemical Geology, v. 103, p. 1–16.

Dagallier, G., Laitnen, A.I., Malartre, F., Van Campenhout, I.P.A.M., and Veeken, P.C.H., 2000, Ground penetrating radar application in a shallow marine Oxfordian limestone sequence located on the eastern flank of the Paris Basin, NE France: Sedimentary Geology, v. 130, p. 149–165.

Das, A.K., Chakraborty, R., Cervera, M.L., and de la Guardia, M., 1995, Metal speciation in solid matrices: Talanta, v. 42, p. 1007–1030.

de Baar, H.J.W., Bacon, M.P., Brewer, P.G., and Bruland, K.W., 1985, Rare earth elements in the Pacific and Atlantic oceans: Geochimica et Cosmochimica Acta, v. 49, p. 1943–1959.

DePaolo, D.J., and Wasserburg, G.J., 1976, Inferences about magma sources and mantle structure from variations of $^{143}Nd/^{144}Nd$: Geophysical Research Letters, v. 3, p. 743–746.

Dia, A., Dupré, B., and Allègre, C.J., 1992, Nd isotopes in Indian Ocean sediments used as a tracer of supply to the ocean and circulation path: Marine Geology, v. 103, p. 349–359.

Downes, H., and Duthou, J.L., 1988, Isotopic and trace element arguments for the lower crustal origin of Hercynian granitoids and Pre-Hercynian orthogneiss, Massif Central, France: Chemical Geology, v. 68, p. 291–308.

Duinker, J.C., Van Eck, G.T.M., and Nolting, R.F., 1974, On the behaviour of copper, zinc, iron and manganese, and evidence for mobilization processes in the Dutch Wadden Sea: Netherlands Journal of Sea Research, v. 8, p. 214–239.

Ehrenberg, S.N., Svånå, T.A., Paterson, B.A., and Mearns, E.W., 2000, Neodymium isotopic profiling of carbonate platform strata: correlation between siliciclastic provenance signature and sequence stratigraphy: Sedimentary Geology, v. 131, p. 87–95.

Eisenhauer, A., Meyer, H., Rachold, V., Tütken, T., Wiegand, B., Hansen, B.T., Spielhagen, R.F., Lindemann, F., and Kassens, H., 1999, Grain size separation and sediment mixing in Arctic Ocean sediments: evidence from the strontium isotope systematic: Chemical Geology, v. 158, p. 173–188.

Elderfield, H., and Greaves, M.J., 1982, The rare earth elements in seawater: Nature, v. 296, p. 214–219.

Elderfield, H., and Sholkovitz, E.R., 1987, REE in the pore-waters of reducing nearshore sediments: Earth and Planetary Science Letters, v. 82, p. 280–288.

Elderfield, H., Hawkesworth, C.J., Greaves, M.J., and Calvert, S.E., 1981, Rare earth element geochemistry of oceanic ferromanganese nodules and associated sediments: Geochimica et Cosmochimica Acta, v. 45, p. 513–528.

Emerson, H.S., and Young, A.K., 1995, Method development for the extraction of naturally occurring radionuclides in marine sediments: Science of the Total Environment, v. 173–174, p. 313–322.

Fagel, N., Innocent, C., Gariepy, C., and Hillaire-Marcel, C., 2002, Sources of Labrador Sea sediments since the last glacial maximum inferred from Nd–Pb isotopes: Geochimica et Cosmochimica Acta, v. 66, p. 2569–2581.

Fallon, S.J., White, J.C., and McCulloch, M.T., 2002, *Porites* corals as recorders of mining and environmental impacts: Misima Island, Papua New Guinea: Geochimica et Cosmochimica Acta, v. 66, p. 45–62.

Fanton, K.C., Holmden, C., Nowlan, G.S., and Haid, F.M., 2002, $^{143}Nd/^{144}Nd$ and Sm/Nd stratigraphy of Late Ordovician epeiric sea carbonates: Geochimica et Cosmochimica Acta, v. 66, p. 241–255.

Faure, G., 1986. Principles of Isotope Geology: New York, J. Wiley & Sons, 589 p.

Fiszman, M., Pfeiffer, W.C., and Drude De lacerda, L., 1984, Comparison of methods used for extraction and geochemical distribution of heavy metals in bottom sediments from Sepetiba Bay, R.J. (Brazil): Environment Technology Letters, v. 5, p. 567–575.

Frank, M., 2002, Radiogenic isotopes: tracers of past ocean circulation and erosional input: Reviews in Geophysics, v. 40, DOI: 10.1029/2000RG000094.

Frank, M., O'Nions, R.K., Hein, J.R., and Banakar, V.K., 1999, 60 Myr records of major elements and Pb–Nd isotopes from hydrogenous ferromanganese crusts: reconstruction of seawater paleochemistry: Geochimica et Cosmochimica Acta, v. 63, p. 1689–1708.

Freydier, R., Michard, A., De Lange, G., and Thomson, J., 2001, Nd isotopic compositions of Eastern Mediterranean sediments: tracers of the Nile influence during sapropel S1 formation?: Marine Geology, v. 177, p. 45–62.

Goldstein, S.J., and Jacobsen, S.B., 1987, The Nd and Sr Isotopic systematics of river-water dissolved material: implications for the sources of Nd and Sr in seawater: Chemical Geology, v. 66, p. 245–272.

Goldstein, S.J., and Jacobsen, S.B., 1988, Nd and Sr isotopic systematics of river water suspended material: implications for crustal evolution: Earth and Planetary Science Letters, v. 87, p. 249–265.

Grandjean, P., Cappetta, H., Michard, A., and Albarede, F., 1987, The assessment of REE patterns and $^{143}Nd/^{144}Nd$ ratios in fish remains: Earth and Planetary Science Letters, v. 84, p. 181–196.

Grandjean, P., Cappetta, H., and Albarede, F., 1988, The REE and Nd of 40–70 Ma old fish debris from the west-African platform: Geophysical Research Letters, v. 15, p. 389–392.

Grandjean-Lecuyer, P., Feist, R., and Albarede, F., 1993, REE in old biogenic apatites: Geochimica et Cosmochimica Acta, v. 57, p. 2507–2514.

Guillocheau, F., Robin, C., Allemand, P., Bourquin, S., Brault, N., Dromart, G., Friedenberg, R., Garcia, J.P., Gaulier, J.M., Gaumet, F., Grosdoy, B., Hanot, F., Le Strat, P., Mettraux, M., Nalpas, T., Prijac, C., Rigollet, C., Serrano, O., and Grandjean, G., 2000, Meso–Cenozoic geodynamic evolution of the Paris Basin: 3D stratigraphic constraints: Geodinamica Acta, v. 13, p. 189–246.

Haese, R.R., Wallmann, K., Dahmke, A., Kretzmann, U., Müller, P.J., and Schulz, H.D., 1997, Iron species determination to investigate early diagenetic reactivity in marine sediments: Geochimica et Cosmochimica Acta, v. 61, p. 63–72.

Haley, B.A., Klinkhammer, G.P., and McManus, J., 2004, Rare earth elements in pore water of marine sediments: Geochimica et Cosmochimica Acta, v. 68, p. 1265–1279.

Hall, G.E.M., Vaive, J.E., Beer, R., and Hoashi, M., 1996, Selective leaches revisited, with emphasis on the amorphous Fe oxyhydroxide phase extraction: Journal of Geochemical Exploration, v. 56, p. 59–78.

Henry, P., Delooule, E., and Michard, A., 1997, The erosion of the Alps: Nd isotopic and geochemical constraints on the sources of the peri-Alpine molasse sediments: Earth and Planetary Science Letters, v. 146, p. 627–644.

Holmden, C., Creaser, R.A., Muelenbachs, K., Bergström, S.M., and Leslie, A.S.A., 1996, Isotopic and elemental systematics of Sr and Nd in 454 Ma biogenic apatites: Implications for paleoseawater studies: Earth and Planetary Science Letters, v. 142, p. 425–437.

Innocent, C., Fagel, N., Stevenson, R.K., and Hillaire-Marcel, C., 1997, Sm–Nd signature of modern and late Quaternary sediments from the northwest North Atlantic: implications for deep current changes since the last glacial maximum: Earth and Planetary Science Letters, v. 146, p. 607–625.

Jeandel, C., Bishop, J.K., and Zindler, A., 1995, Exchange of neodymium and its isotopes between seawater and small and large particles in the Sargasso Sea: Geochimica et Cosmochimica Acta, v. 59, p. 535–547.

Keto, L.S., and Jacobsen, S.B., 1987, Nd and Sr isotopic variations of Early Paleozoic oceans: Earth and Planetary Science Letters, v. 84, p. 27–41.

Kitano, Y., Sakata, M., and Matsumoto, E., 1981, Partitioning of heavy metals into mineral and organic fractions in a sediment core sample from Osaka Bay: Oceanographical Society of Japan, Journal, v. 37, p. 259–266.

Koschinsky, A., Winkler, A., and Fritsche, U., 2003, Importance of different types of marine particles for the scavenging of heavy metals in the deep-sea bottom water: Applied Geochemistry, v. 18, p. 693–710.

Lacan, F., and Jeandel, C., 2005, Neodymium isotopes as a new tool for quantifying exchange fluxes at the continent–ocean interface: Earth and Planetary Science Letters, v. 232, p. 245–257.

Liew, T.C., and Hofmann, A.W., 1988, Precambrian crustal component, plutonic associations, plate environment of the Hercynian Fold Belt of central Europe: indications from a Nd and Sr isotopic study: Contribution to Mineralogy and Petrology, v. 98, p. 129–138.

Martin, E.E., and Haley, B.A., 2000, Fossil fish teeth as proxies for seawater Sr and Nd isotopes: Geochimica et Cosmochimica Acta, v. 64, p. 835–847.

Martin, E.E., and MacDougal, J.D., 1995, Sr and Nd isotopes at the Permian/Triassic boundary: A record of climate change: Chemical Geology, v. 125, p. 73–99.

McLennan, S.M., 1989, Rare earth elements in sedimentary rocks: influence of provenance and sedimentary processes, *in* Lipin, B.R., and McKay, G.A., eds., Sedimentary Rocks: Influence of Provenance and Sedimentary Processes: Mineralogical Society of America, p. 169–200.

Michard, A., Gurriet, P., Soudant, M., and Albarede, F., 1985, Nd isotopes in French Phanerozoic shales: external vs. internal aspects of crustal evolution: Geochimica et Cosmochimica Acta, v. 49, p. 601–610.

Morford, J.L., and Emerson, S., 1999, The geochemistry of redox sensitive trace metals in sediments: Geochimica et Cosmochimica Acta, v. 63, p. 1735–1750.

Négrel, P., Grosbois, C., and Kloppmann, W., 2000a, Multi-element chemistry, Rb–Sr and C–O isotopic systematics in labile fraction of suspended matter: the Loire river case (France): Chemical Geology, v. 166, p. 271–285.

Négrel, P., Guerrot, C., Cocherie, A., Azaroual, M., Brach, M., and Fouillac, C., 2000b, Rare earth elements, neodymium and strontium isotopic systematics in mineral waters: evidence from the Massif Central, France: Applied Geochemistry, v. 15, p. 1345–1367.

Négrel, P., Kloppmann, W., Garcin, M., and Giot, D., 2000c, Chronology of fluvial sediments in the Loire river valley over the past 8500 years BP (abstract): Goldschmidt Conference, Oxford. J. of Conference Abstracts, v. 5, n. 2, p. 739.

Ohta, A., and Kawabe, I., 2001, REE(III) adsorption onto Mn dioxide (δ-MnO_2) and Fe oxyhydroxide: Ce(III) oxidation by δ-MnO_2: Geochimica et Cosmochimica Acta, v. 65, p. 695–703.

Palmer, M.R., and Elderfield, H., 1986, Rare earth elements and neodymium isotopes in ferromanganese oxide coatings of Cenozoic foraminifera from the Atlantic Ocean: Geochimica et Cosmochimica Acta, v. 50, p. 409–417.

Pellenard, P., Deconinck, J.F., Marchand, D., Thierry, J., Fortwenglew, D., and Vigneron, G., 1999, Eustatic and volcanic influence during Middle Callovian to Middle Oxfordian clay sedimentation in the eastern part of the Paris Basin: C.R. Académie des Sciences (Paris), Earth and Planetary Science, v. 328, p. 807–813.

Picard, S., Lecuyer, C., Barrat, J.A., Garcia, J.P., Dromart, G., and Sheppard, S.M.F., 2002, Rare earth element contents of Jurassic fish and reptile teeth and their potential relation to seawater composition (Anglo–Paris Basin, France and England): Chemical Geology, v. 186, p. 1–16.

Piepgras, D.J., and Wasserburg, G.J., 1980, Neodymium isotopic variations in seawater: Earth and Planetary Science Letters, v. 50, p. 128–138.

Pin, C., and Duthou, J.L., 1990, Sources of Hercynian granitoids from the French Massif Central: inferences from Nd isotopes and consequences for crustal evolution: Chemical Geology, v. 83, p. 281–296.

Piper, D.Z., 1974, REE in the sedimentary cycle: a summary: Chemical Geology, v. 14, p. 285–304.

Robinson, D.M., DeCelles, P.G., Patchett, P.J., and Garzione, C.N., 2001, The kinematic evolution of the Nepalese Himalaya interpreted from Nd isotopes: Earth and Planetary Science Letters, v. 192, p. 507–521.

Rutberg, R.L., Hemming, S.R., and Goldstein, S.L., 2000, Reduced North Atlantic Deep Water flux to the glacial Southern Ocean inferred from neodymium isotope ratios: Nature, v. 405, p. 935–938.

Schaltegger, U., Stille, P., Rias, N., Piqué, A., and Clauer, N., 1994, Neodymium and strontium isotopic dating of diagenesis and low-grade metamorphism of argillaceous sediments: Geochimica et Cosmochimica Acta, v. 58, p. 1471–1481.

Snape, R.C., Scouller, S.C., Stark, J., Stark, M., Riddle, J., and Gore, D.B., 2004, Characterisation of the dilute HCl extraction method for the identification of metal contamination in Antarctic marine sediments: Chemosphere, v. 57, p. 491–504.

Shields, G., and Stille, P., 2001, Diagenetic constraints on the use of cerium anomalies as palaeoseawater redox proxies: an isotopic and REE study of Cambrian phosphorites: Chemical Geology, v. 175, p. 29–48.

Sutherland, R.A., 2002, Comparison between non-residual Al, Co, Cu, Fe, Mn, Ni, Pb and Zn released by a three-step sequential extraction procedure and a dilute hydrochloric acid leach for soil and road deposited sediment: Applied Geochemistry, v. 17, p. 353–365.

Simien, F., Mattauer, M., and Allègre, C.J., 1999, Nd isotopes stratigraphic record of the Montagne noire (French Massif Central): no significant Paleozoic juvenile inputs and pre Hercynian paleogeography: Journal of Geology, v. 107, p. 87–97.

Stille, P., and Fischer, H., 1990, Secular variation in the isotopic composition of Nd in Tethys seawater: Geochimica et Cosmochimica Acta, v. 54, p. 3139–3145.

Stille, P., Steinmann, M., and Riggs, S.R., 1996, Nd isotope evidence for the evolution of the paleocurrents in the Atlantic and Tethys oceans during the past 180 Ma: Earth and Planetary Science Letters, v. 11, p. 9–19.

Tachikawa, K., Jeandel, C., Vangriesheim, A., and Dupré, B., 1999a, Distribution of rare earth elements and neodymium isotopes in suspended particles of the tropical Atlantic Ocean (EUMELI site): Deep-Sea Research, Part I: Oceanographic Research, v. 46, p. 733–755.

Tachikawa, K., Jeandel, C., and Roy-Barman, M., 1999b, A new approach to the Nd residence time in the ocean: the role of atmospheric inputs: Earth and Planetary Science Letters, v. 170, p. 433–446.

Tachikawa, K., Athias, V., and Jeandel, C., 2003, Neodymium budget in the modern ocean and paleoceanographic implications: Journal of Geophysical Research, v. 108, p. 3254.

Taylor, S.R., and McLennan, S.M., 1985. The Continental Crust; Its Composition and Evolution: Oxford, U.K., Blackwell Scientific Publications, 312 p.

Tricca, A., Stille, P., Steinmann, M., Kiefel, B., Samuel, J., and Eikenberg, J., 1999, Rare Earth Elements and Sr and Nd isotopic compositions of dissolved and suspended loads from small river in the Vosges mountains (France), the Rhine river and groundwater: Chemical Geology, v. 160, p. 139–158.

Usero, J., Gamero, M., Morillo, J., and Gracia, I., 1998, Comparative study of three sequential extraction procedures for metals in marine sediments: Environment International, v. 24, p. 487–496.

Vance, D., and Burton, K., 1999, Neodymium isotopes in planktonic foraminifera: a record of the response of continental weathering and ocean circulation rates to climate change: Earth and Planetary Science Letters, v. 173, p. 365–379.

Van Valin, R., and Morse, J.W., 1982, An investigation of methods commonly used for the selective removal and characterization of trace metals in sediments: Marine Chemistry, v. 11, p. 535–564.

Vieillard, P., Ramirez, S., Bouchet, A., Cassagnabère, A., Meunire, A., and Jacquot, E., 2004, Alteration of the Callovo–Oxfordian clay from Meuse–Haute Marne Underground Laboratory (France) by alkaline solution: II, modelling of mineral reactions: Applied Geochemistry, v. 19, p. 1699–1709.

Wang, K., Chatterton, B.D.E., Attrep, M., Jr., and Orth, C.J., 1993, Late Ordovician mass extinction in the Selwyn Basin, northwestern Canada: geochemical, sedimentological, and paleontological evidence: Canadian Journal of Earth Sciences, v. 30, p. 1870–1880.

Wang, Y.L., Liu, Y.G., and Schmitt, R.A., 1986, Rare earth element geochemistry of South Atlantic deep sea sediments: Ce anomaly change at ~ 54 My: Geochimica et Cosmochimica Acta, v. 50, p. 1337–1355.

Webb, G.E., and Kamber, B.S., 2000, Rare earth elements in Holocene reefal microbialites: a new shallow seawater proxy: Geochimica et Cosmochimica Acta, v. 64, p. 1557–1565.

Whittaker, S.G., and Kyser, T.K., 1993, Variations in the neodymium and strontium isotopic composition and REE content of molluscan shells from the Cretaceous Western Interior seaway: Geochimica et Cosmochimica Acta, v. 57, p. 4003–4014.

Worash, G., and Valera, R., 2002, Rare earth element geochemistry of the Antalo Supersequence in the Mekele Outlier (Tigray region, northern Ethiopia): Chemical Geology, v. 182, p. 395–407.

Wright, H.S., and Holser, W.T., 1987, Paleoredox variations in ancient oceans recorded by rare earth elements in fossil apatite: Geochimica et Cosmochimica Acta, v. 51, p. 631–644.

Yokoo, Y., Nakano, T., Nishikawa, M., and Quan, H., 2004, Mineralogical variation of Sr–Nd isotopic and elemental compositions in loess and desert sand from the central Loess Plateau in China as a provenance tracer of wet and dry deposition in the northwestern Pacific: Chemical Geology, v. 204, p. 45–62.

Ziegler, P.A., 1988. Evolution of the Arctic–North Atlantic and the Western Tethys: American Association of Geologists, Memoir 43, 198 p.

Received 21 April 2004; accepted 25 August 2005.